Available online at www.sciencedirect.com

SCIENCE DIRECT®

Cement and Concrete Research 35 (2005) 671–679

CEMENT AND CONCRETE RESEARCH

Aggregate–cement paste transition zone properties affecting the salt–frost damage of high-performance concretes

Andrzej Cwirzen*, Vesa Penttala

Laboratory of Building Materials Technology, Helsinki University of Technology, P.O. BOX 2100, FIN-02015 HUT, Finland

Received 11 April 2003; accepted 4 June 2004

Abstract

The influence of the cement paste–aggregate interfacial transition zone (ITZ) on the frost durability of high-performance silica fume concrete (HPSFC) has been studied. Investigation was carried out on eight non-air-entrained concretes having water-to-binder (W/B) ratios of 0.3, 0.35 and 0.42 and different additions of condensed silica fume. Studies on the microstructure and composition of the cement paste have been made by means of environmental scanning electron microscope (ESEM)-BSE, ESEM-EDX and mercury intrusion porosimetry (MIP) analysis. The results showed that the transition zone initiates and accelerates damaging mechanisms by enhancing movement of the pore solution within the concrete during freezing and thawing cycles. Cracks filled with ettringite were primarily formed in the ITZ. The test concretes having good frost–deicing salt durability featured a narrow transition zone and a decreased Ca/Si atomic ratio in the transition zone compared to the bulk cement paste. Moderate additions of silica fume seemed to densify the microstructure of the ITZ.

Keywords: High-performance concrete; Freezing and thawing; Interfacial transition zone; EDX

1. Introduction

Several research groups have studied the interfacial transition zone (ITZ) between cement paste and aggregate. Farran [1] was one of first to observe and describe transition zones surrounding large aggregate particles. Transition zone is roughly 50 μm thick with less dense hydration products. Later, other researchers [2,3] using SEM-EDX described ITZ as having thin film of CH and elongated C-S-H particles depleted on the aggregates. Others [4–6] observed increased concentrations of CH, ettringite and Hadley's grains, as well as higher capillary porosity close to the aggregates.

Two potential mechanisms responsible for existence of the transition zone have been proposed. First, the influence of the so-called wall effect was extensively studied by Maso [7] and Scrivener and Pratt [8]. The results showed that, due to the aggregates, the spatial arrangements of anhydrous cement particles become loose near the aggregate surface. As a result, the local W/C ratio and the porosity tended to be higher, and at the same time, W/C ratio in the bulk cement paste becomes lower. Goldman and Bentur [9] proposed a second mechanism claiming that microbleeding under the aggregates during vibration could also be responsible for the ITZ. Thickness of the ITZ has been estimated by different methods. Scrivener and Pratt [10] developed analysis of the SEM-BSE images while Snyder et al. [11] used mercury intrusion porosimetry (MIP). Their results indicated that the thickness of the ITZ was 35–45 μm depending on the type of concrete and usage of additional binders, e.g., silica fume or fly ash. Most recently, Scrivener and Nemati [12] studied polished specimens impregnated under load with Wood's metal by SEM. Results showed high connectivity and preferential permeability of the ITZ compared to the bulk paste. Due to the increased porosity, the transition zone is considered to influence the transport processes in the concrete. Delagrave et al. [13] studied the influence of ITZ on the chloride diffusivity of mortars. It was found that the presence of aggregates modified considerably the microstructure of the cement paste by introducing transition zones and thus facilitating movement of the chloride ions. Others, e.g., Bourdette et al. [14], stated that the diffusion coefficient of chloride ions can be 6–12 times greater in the transition zone compared to the bulk paste.

* Corresponding author. Tel.: +358-50-352-5675; fax: +358-9-451-3826.
E-mail address: cwirzen@rakserver.hut.fi (A. Cwirzen).

0008-8846/$ – see front matter © 2004 Elsevier Ltd. All rights reserved.
doi:10.1016/j.cemconres.2004.06.009

Table 1
Mix proportions, air content and compressive strength properties of the test concretes

Test concrete	W/B	Silica fume (% of cement content)	Fresh mix air content (%)	Compressive strength (MPa), 100-mm cubes
0.3-0SF	0.3	0	1.6	120
0.3-3SF	0.3	3	1.2	128.3
0.3-7SF	0.3	7	1.8	129.2
0.35-0SF	0.35	3	0.9	109.1
0.35-7SF	0.35	7	1.6	119.1
0.42-0SF	0.42	0	1.6	97.6
0.42-3SF	0.42	3	1.4	97.2
0.42-7SF	0.42	7	1.8	105.4

Consequently, the ITZ—due to its nature—facilitates ingress of external agents and thus supports various deleterious chemical reactions. Furthermore, increased portlandite content may lead to leaching of $Ca(OH)_2$ and the lowering of concrete resistance to ion penetration. For example, enhanced transport processes may begin or accelerate frost damage mechanism.

Despite the investigations already made on the ITZ, some aspects, especially concerning the frost damage, are still unclear. This paper deals primarily with the influence of the ITZ on the internal damage and the surface scaling of high -performance concretes subjected to freezing and thawing cycles in the presence of deicing salts. The investigated mixes were produced by using three water-to-binder (W/B) ratios: 0.3, 0.35 and 0.42. The compressive strengths of the test concretes measured after 28 days were from 97.6 to 129.2 MPa (100 mm cubes). The results of the investigation are hoped to help to better understand the role of the ITZ in frost damage of concrete mechanism.

2. Test concretes

The tested specimens belong to the class of high-performance concretes in which different additions of condensed silica fume was applied. Fresh and hardened concrete properties are presented in Table 1. Rapid hardening Portland cement type CEM I 52.5R produced by Aarlborg Portland was used. Condensed silica fume slurry having the trade name of SF-Centrilin contained 50% of solids and it was added during mixing. Silica fume dosages were 3% and 7% of the cement weight. Polycarboxylate-based superplasticizer MURPLAST FK65 was used. No air entrainment was applied. Mineralogical composition of aggregates was mainly basalt. The consistency of the fresh mix was assessed by the flow table test. The 28-day compressive strengths varied from 97.2 to 129.2 MPa. The specimens were cured for 6 days in water and thereafter preserved in 20 °C and 65% RH until the age of 28 days.

3. Test procedures

Assessment of the frost–salt durability has been done by means of CDF [15] test procedure. Testing was continued up to 56 freezing and thawing cycles. The freezing medium was 3% NaCl solution.

The microstructure of the test samples was studied by using MIP, environmental scanning electron microscope (ESEM) by means of backscattered electron images (BSE) and indirectly by X-rays analysis (EDX). Tests were performed on 28-day-old specimens. In the ESEM-BSE and ESEM-EDX investigations, polished specimens were used. The preparation procedure basically followed recommendations by Detwiler et al. [16]. The test samples of $10 \times 10 \times 2$ mm were cut from $10 \times 10 \times 10$ cm cubes in such a way that the investigated surface was perpendicular to the top surface of the cube. Storage in alcohol for 24 h proceeded resin impregnation under vacuum. In the last stage, specimens were grinded and polished with diamond paste. The flatness of the polished surfaces has been evaluated by atomic force microscope (AFM) and the results showed that the average variation in height of a 70×70 μm specimen area did not exceed 1.5–2 μm. No bigger deviations have been observed in the vicinity of the aggregates. ESEM-BSE analysis was done using magnifications of 500 and 1000. The operating parameters of the ESEM were accelerating voltage 20 keV, chamber pressure 1.8 Torr and working distance 13.3 mm (including ESD detector, which is 10 mm long). Images were analysed with Kevex software to obtain porosity distribution as function of the distance from the aggregate. To enhance contrast between various phases and to separate pores, all images were processed with a Gaussian filter. Phase separation was made according to the procedure proposed by Scrivener and Pratt [17] by using grey level histograms.

Measuring procedure for the ESEM-EDX included spot analysis made in the ITZ and in the bulk cement paste

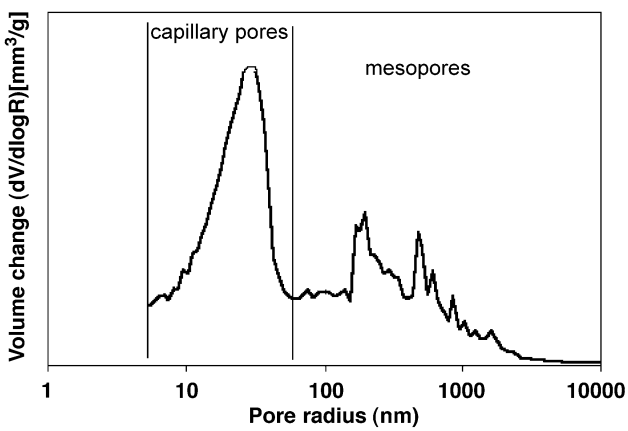

Fig. 1. Definition of the capillary and mesopore range used for MIP analysis.

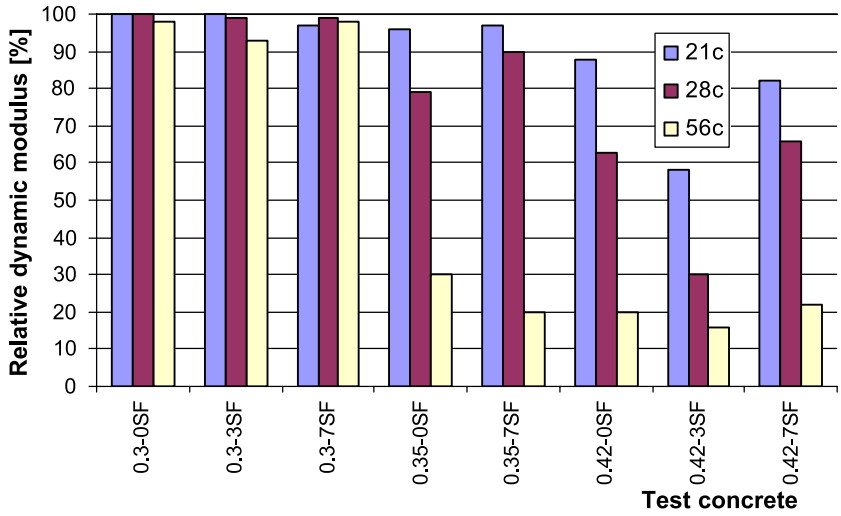

Fig. 2. Internal damage of the test concretes in the CDF-test measured after 21, 28 and 56 freeze–thaw cycles expressed as a function of the relative dynamic modulus of elasticity.

(distance >100 μm from the aggregate) in at least two different locations. Only C-S-H phase has been analysed. Altogether, 20 analyses were performed on each specimen The counting rate of the analyser was kept at around 1500 cps with counting time of 60 s. Quantitative analysis with standards was used. The almandine garnet, albeit and anhydrite standards spectra were recorded before the first analysis was performed. Matrix correction was made by the ZAF procedure. Quantitative analyses were made for Na, Mg, Al, Fe, S, Ca, Si, Mn and K while oxygen was calculated stoichiometrically.

To analyse pore size distribution of the bulk material by means of MIP, pores were divided according to Penttala [18] into capillary and meso ranges (see Fig. 1).

4. Freezing and thawing results

Results of the freeze–thaw tests are presented in Figs. 2 and 3. None of the test concretes having W/B ratio of 0.35 and 0.42 had surface scaling results under 1500 g/m^2 and the dynamic modulus of elasticity (measured by means of the transit time) was less than 60% after 56 cycles (100% denotes no damage). Scaling decreased with increasing silica fume amount and decreasing W/B. The weakest concrete with respect to surface scaling appeared to be concrete having W/B ratio of 0,42 without any silica fume addition. Internal damage was in line with the surface scaling except for the mix 0.42-3SF (W/B ratio 0.42 and 3% silica fume of cement weight). Surprisingly, internal

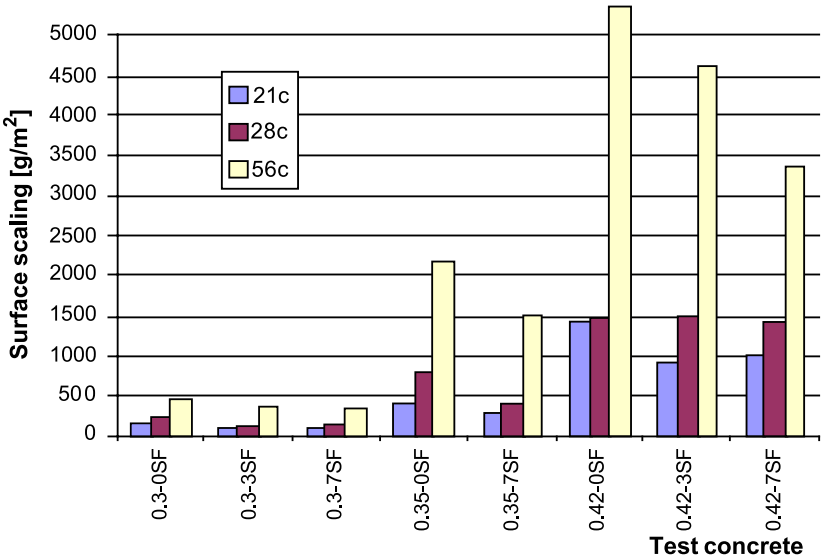

Fig. 3. Surface scaling of the test concretes in the CDF-test after 21, 28 and 56 freeze–thaw cycles.

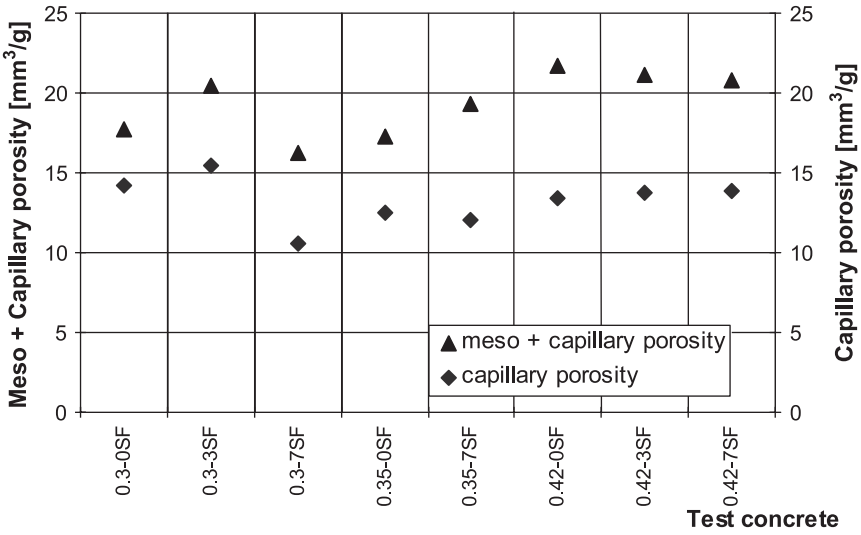

Fig. 4. The sum of meso and capillary porosities and capillary porosity of the test concretes measured from the MIP test results. The porosity values are measured by MIP in the range of pores from 5 to approximately 25,000 nm.

damage for this particular concrete was most severe despite the use of silica fume.

Neither internal damage nor surface scaling was observed for mixes having a W/B ratio of 0.3.

5. Microstructure

The results obtained from MIP investigation presented in Fig. 4 did not show significant variations of total porosity. The concrete having a W/B ratio of 0.3 had an approximately 2% decrease of capillary porosity when silica fume was used. However, for W/B ratios of 0.35 and 0.42, capillary and total porosities appeared to be quite similar.

Fig. 5 shows the results obtained from the BSE images with respect to porosity. To obtain porosity changes, each pixel of the image has been checked for the presence of the pore (black color after thresholding). Observations showed a large increase of capillary porosity from 5% to 9% in the bulk paste to 25% in the ITZ for mixes having W/B ratios of 0.35–0.42. The width of the transition zone varied from 30 to 50 μm (see Figs. 5 and 6). No such changes were observed for mixes having W/B ratios of 0.3. Areas of increased capillary porosity were observed near the surface of the larger aggregate particles and between two or more aggregate particles when the distance between them was less then 50 μm. This suggests that microbleeding has occurred in the fresh state, similarly as Goldman and Bentur [9] has proposed.

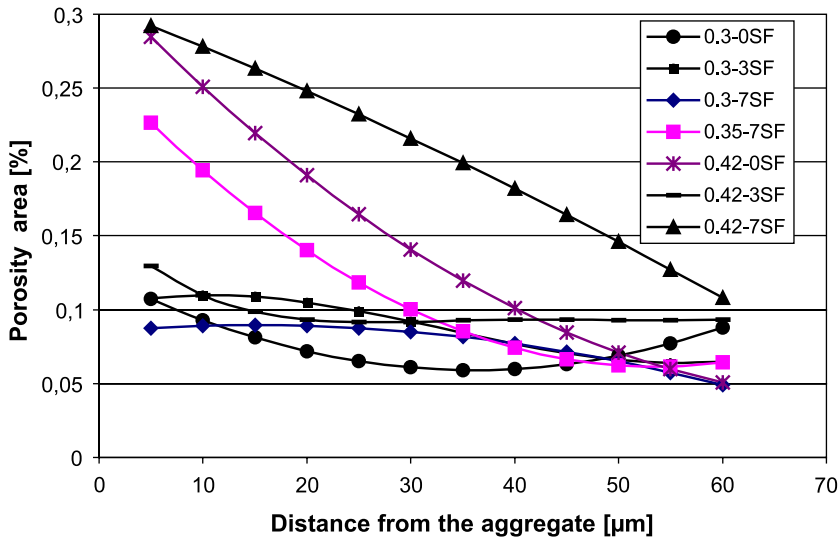

Fig. 5. Capillary porosity data as a function of the distance from the aggregate surface. In this figure, capillary porosity is defined as the porosity detectable in the ESEM-BSE mode measured on the polished specimens.

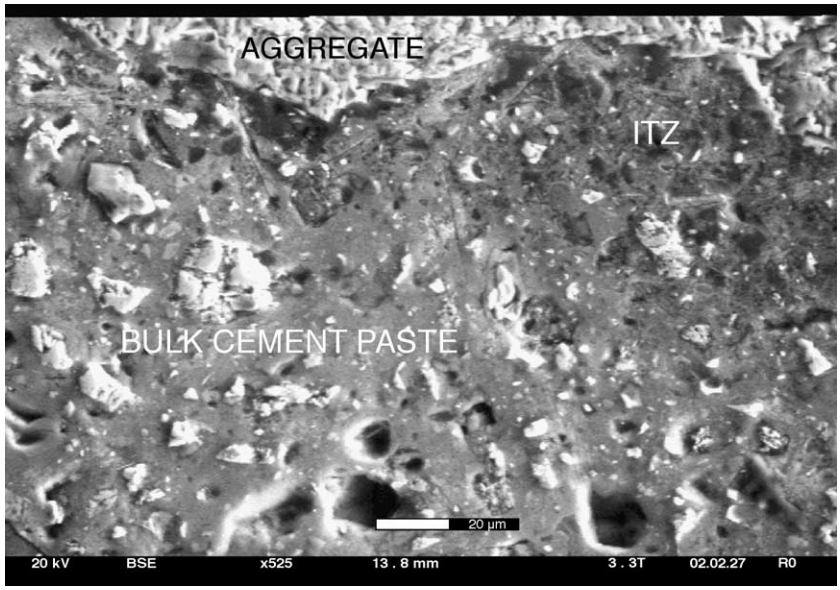

Fig. 6. ESEM-BSE image of the test concrete 0.42-7SF. An ITZ having a width of approximately 30 μm is visible near the aggregate particle as area of increased capillary porosity.

In every mix, no increased amounts of $Ca(OH)_2$, AFt or AFm phases were observed neither in the bulk cement paste nor in the ITZ in the BSE images. Some agglomerates of silica fume could be detected, although without any preferences in location. No microcracks were detected at the magnification of 1000 times in the cement paste of any of the studied concretes. Additional ESEM-SE (secondary electron mode) studies were done on some of the test concretes which had deteriorated during freeze–thaw cycles. In these tests, fractured unpolished specimens were used. In all studied cases, formations of ettringite-like needles in pores and cracks were observed (see Fig. 7).

Results from ESEM-EDX analysis are presented in Fig. 8. Statistical analysis using *t* test and Kolmogrov–Smirnof test has been performed to check statistical significance of the recorded differences of the atomic ratios between ITZ and bulk cement paste. The test concretes having such differences have been underlined. In general, Ca/Si atomic ratio measured in the bulk cement paste decreased with increasing W/B ratio and, in most cases, decreased also

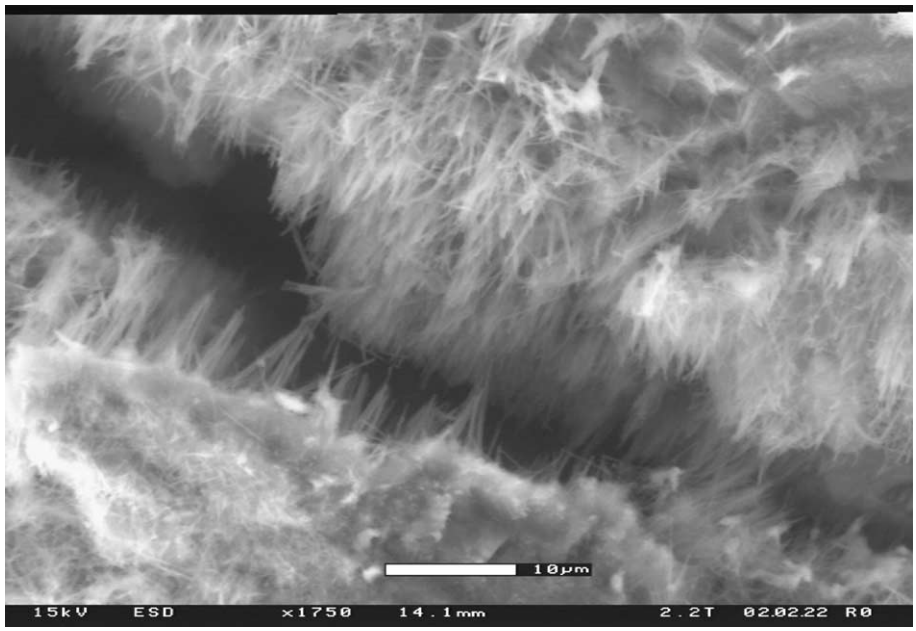

Fig. 7. ESEM-EDS image of a crack in which ettringite needles are visible after 56 freezing and thawing cycles in the presence of deicing salts. Test concrete was 0.42-7SF.

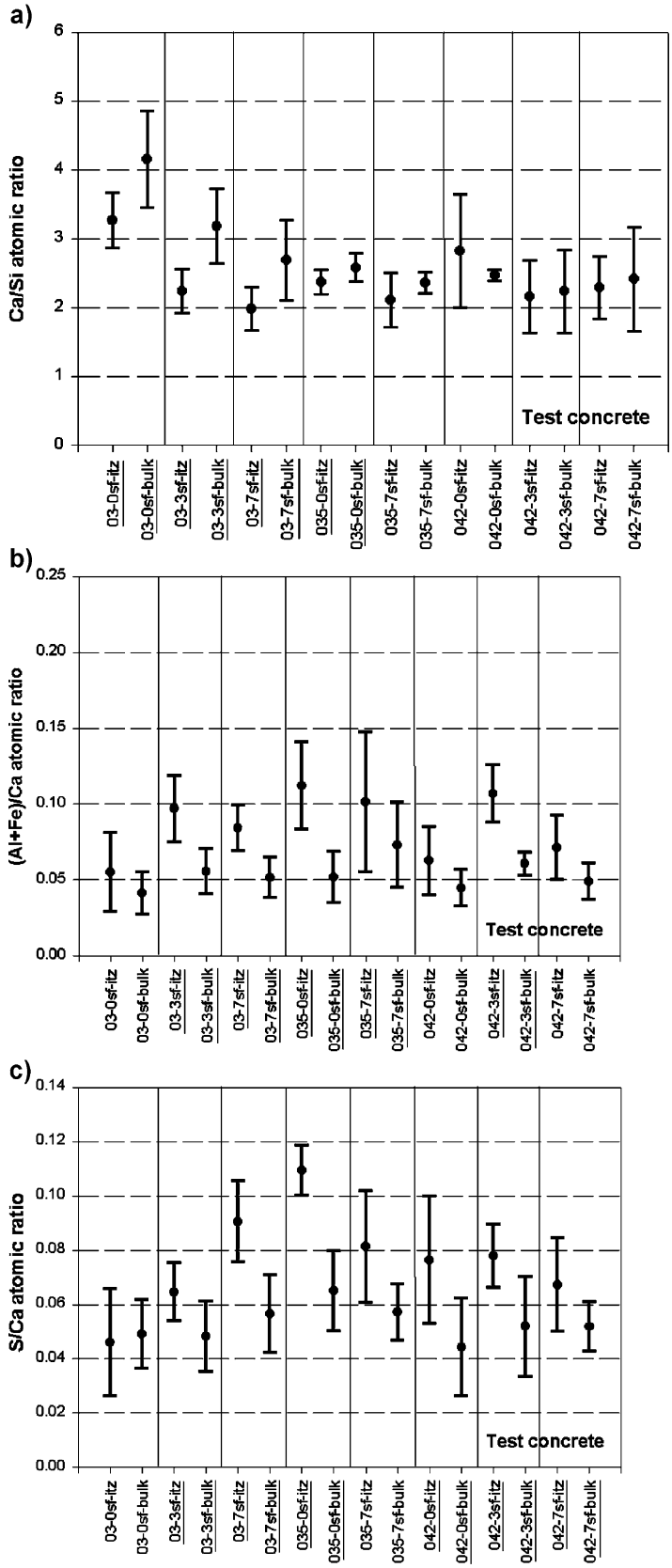

Fig. 8. Average atomic ratios and corresponding standard deviations of the ITZ and bulk binder paste measured by ESEM-EDX: (a) Ca/Si, (b) (Al + Fe)/Ca and (c) S/Ca. When there is a statistical difference of the atomic ratios between ITZ and bulk cement paste, the test concrete has been underlined.

when silica fume content increased. Remarkable differences could be observed between ITZ and bulk cement paste. Mixes having a W/B ratio of 0.3 showed a large decrease of the Ca/Si ratio in the vicinity of the aggregates, e.g., for mix 0.3-7SF, from 2.59 to 1.98. This tendency became more obvious with increasing SF content. Mixes having W/B ratios of 0.35 and 0.42 showed small differences or a small increase of this ratio, e.g., in mix 0.42-0SF. However, this could not be proved statistically. The (Al + Fe)/Ca and S/Ca atomic ratios showed a slight increase in the ITZ. Addition of SF did not have remarkable influence on these ratios.

6. Discussion

Assuming that aggregates are not subjected to any form of deterioration either due to the frost attack or chloride penetration, the composition and microstructure of the cement paste determine the frost durability of the test concretes. Presented studies showed that concretes having a low W/B ratio (0.3) have a very dense and homogeneous microstructure of the cement paste. BSE investigation of these concretes confirmed the existence of a barely detectable transition zone (< 5 μm wide). In the contrary, concretes of higher water content (W/B ratio of 0.35 and 0.42) appeared to be less homogeneous. The transition zone was clearly visible in the BSE images reaching a transition zone width of 30–40 μm and a porosity increase from 10% to 25% could be noticed (see Fig. 5). Slightly narrower ITZ width could be observed when silica fume was used. Similar results were obtained by Kjellsen et al. [6], who observed 40-μm-wide ITZ in concrete having a W/C ratio of 0.4. These observations could be directly related to the results of the freeze–thaw tests. The concretes featuring narrow transition zone appeared to have a low surface scaling of less then 500 g/m^2 and internal damage at around 90% measured by relative dynamic modulus. The concretes having a wide and porous ITZ deteriorated severely. The results indicate that ITZ, due to its connectivity, has enhanced penetration of the freezing medium. Furthermore, water uptake was increased by a pumping effect caused by freezing and thawing cycles, as Setzer [15] and Penttala and Al-Neshawy [19] have shown.

The ESEM-SE images of concretes subjected to frost attack (Fig. 7) indicated the presence of ettringite needles in cracks and air voids. Presumably, ettringite appeared as a secondary formation through recrystallization [20,21]. The higher porosity of ITZ could enhance the transport processes of pore liquids, thus allowing frequent moisture changes and permanent high water supply in the transition zone. Furthermore, increased amounts of Al, Fe and S ions in the transition zone (Fig. 5) supported the release of sulphates needed for recrystallization. The presence of the deicing salts, according to Stark and Bollmann [20], can cause partial transformation of monosulphate to Fridel's salts, releasing gypsum, which subsequently reacts with remaining monosulphate to form ettringite. Moreover, the higher diffusivity coefficient in the ITZ could additionally support the entire process. Unfortunately, the results cannot indicate whether ettringite was the cause of crack formation in the ITZ or it just appeared as a secondary deposition. In the authors' opinion, ettringite supports damaging mechanisms indirectly by increasing the capillary water uptake, proposed also by Stark and Bollmann [20].

EDX analysis confirmed discrepancies of Ca/Si atomic ratio between the transition zone and the bulk cement paste, observed also by Larbi and Bijen [5]. The concretes having high W/B ratios (0.42) revealed increase of the CaO content in the ITZ, while in the test concretes having a low W/B ratio (0.3), a significant decrease was detected. This decrease was more pronounced for mixes with silica fume, which, due to the pozzolanic reactions, reacted with $Ca(OH)_2$ and formed more C-S-H gel. At the same time, the total Ca/Si ratios were higher in concretes having low W/B ratios, observed also by Kjellsen et al. [6] and Taylor [22]. This confirms the tendency that $Ca(OH)_2$ tends to be more finely dispersed and intermixed with C-S-H phase in concretes having low W/B ratios.

Concerning EDX spot analysis, it can be noticed that due to the limitations of the method, the measured atomic ratios do not express the real values for C-S-H phase. The main reason for this is that in order to limit the spreading of the electron beam, acceleration voltage of the microscope must be kept at a high level of 20 keV, described by Mathieu [23]. As a result, X-ray-interacting volume can reach even several micrometers. Therefore, it is not possible to ensure absence of other phases, e.g., portlandite, gel or capillary pores, unhydrated cement particles or aggregates, which could be beneath the observed surface of the specimen. For this reason, measured atomic ratios must be treated with caution and considered as an average chemical composition of the analysed bulk of the material.

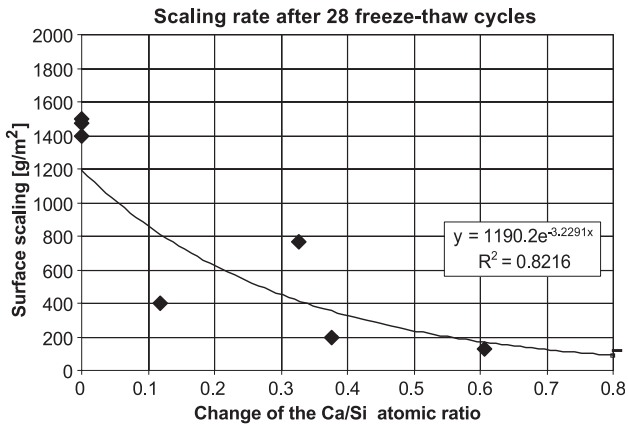

Fig. 9. Relation between the surface scaling after 28 freezing–thawing cycles and change of the Ca/Si atomic ratio calculated as the difference between Ca/Si ratio measured in the bulk cement paste and in the transition zone. Higher change means lower Ca/Si ratios in the ITZ.

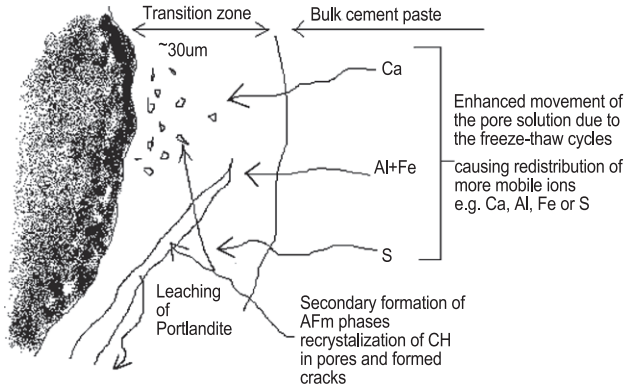

Fig. 10. Diagram representing phenomena taking place in the transition zone during freeze–thaw cycles.

To determine the influence of the aggregates on the EDX analysis, tests with the cement paste have been made. Results did not show any significant discrepancies between the values recorded in cement paste and concrete specimens. Besides, all values for the Ca/Si atomic ratio were somewhat higher when compared with relevant results obtained from bulk cement paste in concrete.

Analysis of the results showed that the test concretes, which revealed the decrease of the Ca/Si ratio in the transition zone, showed improved resistance in the frost deicing salt attack (Fig. 9).

This relation indicates a more homogenous microstructure of the cement paste in the transition zone by means of lower capillary porosity, fewer portlandite crystals, and most probably, less AFt/m phases intermixed with C-S-H. As a result, transport processes and ingress of the freezing medium have been considerably reduced, consequently decreasing the surface scaling.

On the other hand, no direct relations have been found between the results of the freeze–thaw tests and the changes in (Al+Fe)/Ca and S/Ca atomic ratios within the cement paste of the tests concretes. Fig. 10 shows the proposed mechanism, which could be considered as contributing to the frost deicing salts' damage of concrete. The diagram takes into account the results obtained from studies of the microstructure and chemistry of the test concretes.

7. Conclusions

The influence of the transition zone on the frost durability of high-performance concretes has been studied. The non-air-entrained high-performance concretes were produced by 0%, 3% and 7% additions of condensed silica fume by the cement weight. The compressive strength of the test concretes varied from 97.6 to 126.2 MPa (100 mm cubes).

In agreement with previous findings, the ITZ around larger aggregate particles was characterised by a higher capillary porosity, larger calcium hydroxide amount and fewer unhydrated cement particles compared to the bulk cement paste. Lowering the W/B ratio decreased the width of the ITZ from 40 μm (W/B ratio of 0.42) to less than 5 μm (W/B ratio 0.30). Silica fume slightly lowered the content of the Ca/Si atomic ratio in the ITZ. Freeze–thaw durability of concretes having low W/B ratio was good. For all studied concretes, the surface scaling could be directly related to the microstructure and composition of the ITZ. The data obtained from MIP did not correlate with freeze–thaw durability. The concretes having low surface scaling had a barely detectable (<5 μm) transition zone and a decreased content of portlandite in the ITZ. This conclusion was drawn from the Ca/Si atomic ratio results produced by EDX-analysis. In all test concretes having higher W/B ratios (0.35 and 0.42) and wide, porous and CH-rich transition zone, freeze–thaw deterioration was observed.

In general, results indicate that transition zone properties govern the damaging processes of non-air-entrained high-performance concretes by enhancing transport processes within the concrete and facilitating ingress and penetration of the freezing medium and aggressive agents into the concrete microstructure. The chemical composition and higher porosity of the ITZ enhance the secondary formations of AFt phases and leaching of the portlandite.

Further research is needed to cover a wider range of the W/B ratios and higher additions of silica fume.

References

[1] J. Farran, Contribution mineralogique a l'etude de l'adherence entre les constiuants hydrates des cifments et les materiaux enrobes, Rev. Mater. Constr., (490-91) (1956) 155–172.
[2] D. Hadley, The nature of the paste–aggregate interface, PhD thesis, Purdue University, 1972.
[3] B.D. Barnes, S. Diamond, W.L. Dolch, Micromorphology of the interfacial zone around aggregates in Portland cement mortar, Am. Ceram. Soc. 62 (1–2) (1979) 21–24.
[4] A.W. Pope, H.M. Jennings, The influence of the mixing on the microstructure of the cement paste/aggregate interfacial transition zone and on strength of mortar, J. Mater. Sci. 27 (1992) 6452–6462.
[5] J.A. Larbi, J.M.J.M. Bijen, Effects of the water–cement ratio, quality and finesse of sand on the evolution of like in set Portland cement systems, Cem. Concr. Res. 20 (1990) 783–794.
[6] K.O. Kjellsen, O.H. Wallevik, L. Fjallberg, Microstructure and microchemistry of the paste–aggregate interfacial zone of high performance concrete, Adv. Cem. Res. 10 (1) (1998) 30–40.
[7] J.C. Maso, The bond between aggregates and hydrated cement pastes, Proceedings of the 7th International Cement Congress, 1980, pp. 3–15.
[8] K. Scrivener, P.L. Pratt, RILEM TC 108 State of the Art Report, New York, 1994.
[9] A. Goldman, A. Bentur, Effects of pozzolanic and non-reactive microfillers on the transition zone in high strength concretes, in: J.C. Maso (Ed.), Proceedings of the RILEM International Conference (Toulouse), Proceedings 18, Interfaces in Cementitious Composites, E&FN Spon, London, 1992, pp. 53–61.
[10] K.L. Scrivener, P.L. Pratt, A preliminary study of the microstructure of the cement/sand bond in mortars, Proceedings of the 8th International Congress of the Chemistry of Cement, Rio de Janeiro, 1986, pp. 466–471.
[11] K.A. Snyder, D.N. Winslow, D.P. Bentz, E.J. Garboczi, Interfacial

zone percolation in cement–aggregate composites, in: J.C. Maso (Ed.), Proceedings of the RILEM International Conference (Toulouse), Proceedings 18, Interfaces in Cementitious Composites, E&FN Spon, London, 1992, pp. 259–268.
[12] K.L. Scrivener, K.M. Nemati, The percolation of pore space in the cement paste/aggregate interfacial transition zone of concrete, Cem. Concr. Res. 26 (1) (1996) 35–40.
[13] A. Delagrave, J.P. Bigas, J.P. Ollivier, J. Marchand, M. Pigeon, Influence of the interfacial transition zone on the chloride diffusivity of mortars, Adv. Cem. Based Mater. 5 (1997) 86–89.
[14] B. Bourdette, E. Ringot, J.P. Ollivier, Modelling of the transition zone porosity, Cem. Concr. Res. 25 (4) (1995) 741–751.
[15] M.J. Setzer, Action of frost and de-icing chemicals, basic phenomena and testing, RILEM Proceedings vol. 30, (1997) 2–22.
[16] R.J. Detwiler, L.J. Powers, U. Hjorth Jackobsen, W.U. Ahmed, K.L. Scrivener, K.O. Kjellsen, Preparing specimens for microscopy, Concr. Int., (2001 November) 51–58.
[17] K.L. Scrivener, P.L. Pratt, The characterisation and quantification of cement and concretes microstructures, Proceedings of the First International RILEM Congress on Pores Structure and Materials Properties, Versailles, France, 1987, pp. 61–68.
[18] V. Penttala, Effects of microporosity on the compression strength and freezing durability of high-strength concretes, Mag. Concr. Res. 41 (148) (1989) 171–181.
[19] V. Penttala, F. Al-Neshawy, Stress and strain state of concrete during freezing and thawing cycles, Cem. Concr. Res. 32 (2002) 1407–1420.
[20] J. Stark, K. Bollmann, Ettringite formation—A durability problem of concrete pavements, Proceedings of the 10th ICCC Gothenburg, Sweden vol. IV, (4iv062, 8 pp.).
[21] J. Stark, H.M. Ludwig, The influence of the type of cement on the freeze–thaw/freeze–de-icing salt resistance of concrete, Proceedings of the International Conference on Concrete Under Severe Conditions, Sapporo, Japan, 1995, pp. 245–254.
[22] H.F.W. Taylor, Cement Chemistry, 2nd ed., Reedwood Books, Trowbridge, 1997.
[23] C. Mathieu, The beam–gas and signal–gas interactions in the variable pressure scanning electron microscope, Scan. Microsc. 13 (1) (1999) 23–41.